RSC Advances

PAPER

View Article Online
View Journal | View Issue

Cite this: *RSC Adv.*, 2020, **10**, 35039

Are disulfide bonds resilient to double ionization? Insights from coincidence spectroscopy and *ab initio* calculations†

Lautaro R. Varas, *[a] Felipe Fantuzzi, [bcd] Lúcia Helena Coutinho, [e] Rafael B. Bernini, [f] Marco Antonio Chaer Nascimento [b] and G. G. B. de Souza*[b]

Disulfide bonds (–S–S–) are commonly present in biomolecules and have also been detected in astrophysical environments. In this work, the stability of the disulfide bond towards double ionization is investigated using quantum chemical calculations and photoelectron photoion photoion coincidence (PEPIPICO) spectroscopy measurements on the prototype dimethyl disulfide (CH_3SSCH_3, DMDS) molecule. The experiments were performed using high energy synchrotron radiation photons before (2465.0 eV) and at (2470.9 eV) the first sigma resonance around the S 1s edge. We applied the multivariate normal distribution analysis to identify the most plausible ionic fragmentation mechanisms from the doubly ionized DMDS. By mapping the minimum energy structures on the dicationic $C_2H_6S_2^{2+}$ potential energy surface, we show that disulfide bonds are only present in high-lying isomers, in contrast to their analogous neutral systems. Our results also indicate that the number of fragment ions containing a disulfide bond for both photon energies is negligible. Taken together, our results reveal that the disulfide bond is severely damaged as a consequence of sulfur core–shell ionization processes, due to the lowering of its thermodynamic stability in multiply-charged systems.

Received 8th July 2020
Accepted 14th September 2020

DOI: 10.1039/d0ra05979j

rsc.li/rsc-advances

1 Introduction

Sulfur is one of the most abundant chemical elements in the universe. As a consequence, distinct classes of sulfur-bearing molecules are detected in a variety of astrophysical environments – from protostellar outflows,[1] protoplanetary disks,[2] photodissociation regions[3] and infrared dark clouds[4] to interstellar ice analogs,[5,6] planetary atmospheres[7,8] and meteorites.[9] The element is also considered crucial for the emergence and development of life on Earth. Organosulfur compounds and amino acids, for example, are easily formed in experiments simulating an H_2S-containing prebiotic atmosphere, related to early planetary volcanism.[10,11] It is also the basis of the chemo-autotrophic *iron–sulfur world* origin of life theory developed by Wächtershäuser,[12,13] where the exoergic transformation of FeS into pyrite (FeS_2) in the presence of H_2S is proposed as a key energy-delivering source for early metabolism on primitive Earth.[14]

Similarly to carbon, sulfur makes strong bonds with itself. It is the element with the largest number of solid allotropes, exhibiting a pronounced tendency for catenation.[15,16] A large number of stable S_n clusters have been described by computational[17–20] and experimental[21–24] tools, most of them containing either rings or chains. The octamer S_8 crown ring with D_{4d} symmetry is the most stable S_n cluster,[19] and also the most common species in sulfur melts below the polymerization temperature.[25,26] Additionally, iron–sulfur clusters[27] represent another important class of sulfur-containing molecules, which are present in a variety of metalloproteins with distinct functionalities.[28]

The S_2 unit, the smallest motif containing a sulfur–sulfur chemical bond, is known as the disulfide bond (–S–S–). The first interstellar molecule containing such a feature, S_2H, was only recently observed by Fuente and co-workers[29] in the Horsehead nebula, possibly resulting from the proton detachment of an $HSSH^+$ intermediate.[30] Moreover, the disulfide bond plays a very important role in the stability, solubility and folding of proteins, being present in around 10% of the proteins produced by mammalian cells.[31–35] In some cases, disulfide bonds are also

[a]*Escuela de Ingeniería Química, Universidad de Costa Rica, Ciudad de la Investigación, Facultad de Ingeniería, 4o piso, 11501-2060 San José, Costa Rica. E-mail: lautaro.ramirezvaras@ucr.ac.cr*

[b]*Instituto de Química, Universidade Federal do Rio de Janeiro, Cidade Universitária, Ilha do Fundão, 21949-909, Rio de Janeiro, RJ, Brazil. E-mail: gerson@iq.ufrj.br*

[c]*Institut für Anorganische Chemie, Julius-Maximilians-Universität Würzburg, Am Hubland, 97074 Würzburg, Germany*

[d]*Institut für Physikalische und Theoretische Chemie, Julius-Maximilians-Universität Würzburg, Emil-Fischer-Straße 42, 97074 Würzburg, Germany*

[e]*Instituto de Física, Universidade Federal do Rio de Janeiro, Av. Athos da Silveira Ramos 149, 21941-972, Rio de Janeiro, Brazil*

[f]*Instituto Federal de Ciência e Tecnologia do Rio de Janeiro (IFRJ), Duque de Caxias, 25050-100, RJ, Brazil*

† Electronic supplementary information (ESI) available. See DOI: 10.1039/d0ra05979j

directly involved in the enzyme activity, mediating thiol-disulfide interchange reactions in subsequent oxidation/reduction cycles.[36] The allosteric disulfides[33] comprise a third type of disulfide bond, controlling protein function by triggering conformational changes in the three-dimensional biomolecular structure. Finally, disulfide bonds may also have played a role in non-enzymatic routes for the prebiotic formation of deoxynucleotides.[37] Taken together, these results point out that understanding the stability of the disulfide bond towards external agents, such as radiation, is of crucial interest for biochemical processes, astrochemistry and early Earth studies.

In the past years, our group has been investigating the absorption and ionic fragmentation of sulfur-containing molecules after core electron excitations[38] using synchrotron radiation,[39,40] high-energy electrons[41] and ions.[42] The excitation and ionization of core electrons may lead to breakage of chemical bonds and dissociation of molecules. This is attributed to Auger-type processes, in which relaxation after the core-hole formation leads to the ejection of one (or even more) valence electron(s). As a consequence, a multiply-charged species is formed, usually unstable and possessing dissociative character.

Herein, we focus our attention on dimethyl disulfide (CH_3SSCH_3, DMDS), which can be considered as a prototype for systems containing covalent disulfide bonds. A brief review of valence-shell photoionization of DMDS can be found in Bernini *et al.*[39] Borkar *et al.*[43] discuss the fragmentation, both theoretically and experimentally, at low photon energies (9.5 eV to 14.4 eV) using photoelectron–photoion coincidence (PEPICO) measurements. Single dissociation pathways of DMDS at lower energies were also studied by Butler *et al.*[44] and Chiang *et al.*[45] In a previous work, we investigated the ion–ion coincidence spectrum of DMDS obtained at an incident electron energy of 800 eV (valence-shell study due to the energy transferred after the impact).[46]

In this work, we extend this analysis to high-energy photon impact ($\sim$ 2400 eV). Photoelectron–photoion–photoion coincidence (PEPIPICO) experiments[47,48] were employed in order to investigate the most relevant mechanisms of ionic fragmentation after double ionization starting from excitation around the S 1s edge. For analyzing the PEPIPICO data, we applied a multivariate normal distribution methodology adapted by our group to study coincidence techniques.[46] Additionally, we apply quantum chemical calculations in order to elucidate the structure and relative stability of $C_2H_6S_2^{2+}$ isomers, aiming at investigating the stability of the disulfide bond after production of a doubly ionized dimethyl disulfide. Density functional theory and coupled-cluster calculations were used for mapping the minimum energy geometries of the dicationic $C_2H_6S_2^{2+}$ potential energy surface. A comparison between the most stable doubly-charged species with the neutral ones gives insights on the thermodynamic stability of the S–S linkage after double ionization. Our results are discussed in the context of understanding the radiation damage of sulfur-containing proteins and the survival of species bearing disulfide bonds in astrochemical and prebiotic scenarios.

2 Methods

Initially, we obtained Near Edge X-ray Absorption Fine Structure (NEXAFS) spectra and performed PEPICO measurements around the S 1s edge of DMDS using the Soft X-ray Spectroscopy beamline (SXS) in the Laboratório Nacional de Luz Síncrotron (LNLS), Campinas, Brazil. These results were published in early works of our group[46,49] and will not be discussed herein. Details of the experimental setup are also described elsewhere.[46,49]

At high photon energy regimes, there is a large probability of double (or multiple) ionization, whose molecular states are usually highly dissociative. PEPIPICO experiments were employed to characterize the main ionic fragments from such events. The basic principle of the PEPIPICO technique consists in the detection, following photon absorption, of two positive ions resulting from a single Coulomb explosion process. The start measurement of ions arrival times is provided by the photoelectron.[50] With such measurements it is possible to obtain the component of the ion linear momentum along the spectrometer axis. Depending on the momentum balance, for a limited number of linear and sequenced reactions,[51] it is possible to relate the ion coincidence spectra with the molecular fragmentation mechanism,[48,52] whose dynamics could involve two-, three- and four-body dissociations (for a description of such mechanisms see Simon *et al.*[52]).

In the present study we apply the multivariate normal distribution analysis to identify viable ionic fragmentation mechanisms. A complete description of the method can be found elsewhere.[46] Briefly, the ion–ion coincidence spectrum is considered as a linear combination of Gaussian-type multivariate functions. The full width at half maximum (FWHM) for a Gaussian function is given by:[53]

$$\mathrm{FWHM} = \sigma\sqrt{2\ln 2} \tag{1}$$

The Gaussian probability function only depends on two parameters: the standard deviation (σ) and the expected time-of-flight value (μ) of the mass peaks. According to the momentum balance, a given fragmentation reaction can be described by a system of linear equations. The parameters of this linear system are the FWHM of the mass peaks in the PEPIPICO spectra, which are proportional to the kinetic energy of the ion. Thus, the ratio between the standard deviations are calculated and can be compared with the island slopes (see *e.g.* Eland 1987 (ref. 48)).

The normal density function G_{ij} of each set of i, j ion–ion coincidence peak is expressed as a function of μ and Σ:

$$G_{ij} = \frac{1}{\sqrt{2\pi|\Sigma|}} \times \exp\left\{ -\left[\frac{1}{2}(x-\mu)^{\mathrm{T}}\Sigma^{-1}(x-\mu)\right]\right\} \tag{2}$$

where $\mu = \begin{pmatrix} t_1 \\ t_2 \end{pmatrix}$ is the vector of the expected time values (t_1 and t_2 for the bivariate case) of the projection plot; $x = (t_1, t_2)$ describes the mutually independent time variables; and Σ is the variance–covariance matrix between t_1 and t_2:

$$\Sigma = \begin{pmatrix} t_1 & {\sigma_{t_1}}^2{\sigma_{t_2}}^2 \cos\theta \\ {\sigma_{t_1}}^2{\sigma_{t_2}}^2 \cos\theta & t_2 \end{pmatrix} \quad (3)$$

with ${\sigma_{t_1}}^2$ and ${\sigma_{t_2}}^2$ being the variances of the time vector variables and θ the angle between them. Considering that the probability density function for each dissociation (Coulomb explosion) is given by G_{ij}, the total law of probability, G, considering all dissociation processes, can be expressed as follows:

$$G = \sum_{i,j \geq i}^{k} G_{ij}P_{ij} = G_{11}P_{11} + G_{12}P_{12} + \ldots + G_{kk}P_{kk} \quad (4)$$

the P_{ij} given by the following relation:

$$P_{ij} = \frac{n_{ij}e_{ij}}{\sum n_{ij}e_{ij}} = \frac{n_{ij}e_{ij}}{N_{ij}} \quad (5)$$

The above equation is the relation among all the events in the Coulomb ion–ion explosion spectra, given by N_{ij}, whereas n_{ij} is the number of total counts of a particular ion–ion coincidence (or island) and e_{ij} the detector efficiency of each event. Detection efficiencies and high-order aborted coincidences were taken into account during the data analysis by using a protocol developed by the LNLS team for the TOF spectrometer used in our experiments.[54]

As for the quantum chemical calculations, from thirty different initial structures, geometry optimizations and frequency calculations of the $C_2H_6S_2$ dication at the (U)M06-2X/cc-pVTZ level for singlet and triplet multiplicities were performed. The initial structures were built varying the presence of rings (open-chain or cyclic), the type of chain (straight or branched), the CS bonding arrangement (CCSS, CSCS, CSSC, SCCS), and the position of the hydrogen atoms and formal positive charges. Hessian calculations were only performed for structures with electronic energy in the range of 0–30 kcal mol^{-1} from the least energetic structure. Since this was not the case for any of the triplet species, only singlet geometries were characterized by the frequency analysis. Single-point calculations at the CCSD(T)/aug-cc-pVTZ were performed at the optimized structures. The isomers were organized by their relative enthalpy values at 298 K (H^{298}) in the ascending order (**1** denotes the most stable dication whereas **14** denotes the highest energy isomer described herein). We also studied the thermochemistry of selected dissociation pathways taking the minimum energy structure (**13**) – which most closely resembles the neutral DMDS molecule – as reference. Geometry optimizations and frequency analyses of all fragments were obtained following the same methodology as for $C_2H_6S_2{}^{2+}$. All calculations were performed using the Gaussian 16 program package.[55]

3 Results and discussion

3.1 Structure and stability of $C_2H_6S_2{}^{2+}$ isomers

Fig. 1 shows the formal Lewis structure of the $C_2H_6S_2$ dications in the enthalpy ascending order. The relative enthalpy value of each isomer is shown in parenthesis, in kcal mol^{-1}. Fig. 2, on the other hand, shows the optimized $C_2H_6S_2{}^{2+}$ molecular

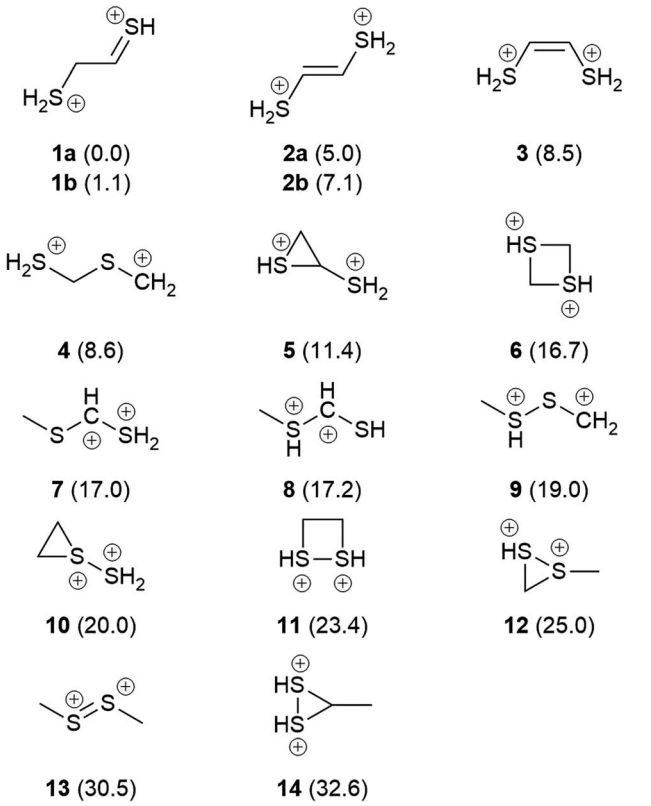

Fig. 1 The most stable $C_2H_6S_2$ dication (**1a**) and its low-lying isomers. The H^{298} values (kcal mol^{-1}) relative to **1a** at the CCSD(T)/aug-cc-pVTZ//M06-2X/cc-pVTZ level of theory are shown in parenthesis.

structures obtained in this work classified by the type of carbon–sulfur skeleton.

The most stable isomers of $C_2H_6S_2{}^{2+}$ are open-chain structures, featuring either SCCS or CSCS skeletons and formal charges at the terminal atoms. **1a** (0.0 kcal mol^{-1}) and **1b** (1.1 kcal mol^{-1}) are two distinct rotamers of an out-of-plane SCCS motif related to the 2-mercaptoethanethial molecule, with protonation at both terminals. This energy difference is close to the expected average errors of CCSD(T)/aug-cc-pVTZ for isomerization energies of organic compounds.[56] The low-lying isomers **2a** and **2b**, on the other hand, lay 5.0 and 7.1 kcal mol^{-1} above **1a**. While for the former species the bond distances suggest the presence of a carbon–sulfur double bond in one of the terminals and a single sp^3–sp^2-like carbon–carbon central bond (**1a:** C–C = 1.495 Å; C=S = 1.624 Å), for **2a** and **2b** a central carbon–carbon double bond (**2a:** C=C = 1.320 Å) and terminal single C–S bonds (1.802 Å) are observed. This set of rotamers are related to the *trans*-ethylenedithiol molecule, protonated at both SH terminal groups. The next low-lying isomer (**3**, 8.5 kcal mol^{-1}) is also analogous to the ethylenedithiol molecule, but in a *cis*-type configuration. Isomer **4** (8.6 kcal mol^{-1}) is the most stable one in which a primary carbon is at the terminal of a straight chain. This structure is related to the mercaptomethylthiomethylium ion, protonated at the terminal SH. Other straight chain isomers containing one

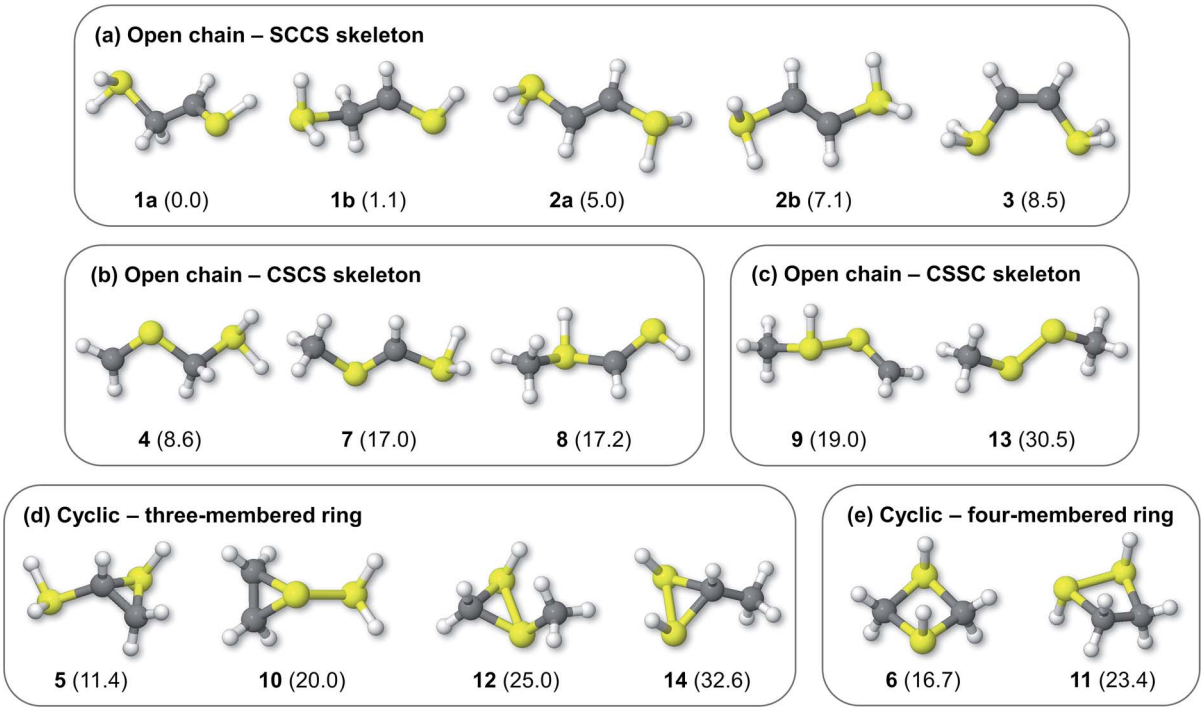

Fig. 2 Optimized $C_2H_6S_2^{2+}$ structures bearing open chain (a) SCCS, (b) CSCS, and (c) CSSC skeleton bonding motifs, and cyclic (d) three- and (e) four-membered rings. The H^{298} values (kcal mol^{-1}) relative to **1a** at the CCSD(T)/aug-cc-pVTZ//M06-2X/cc-pVTZ level of theory are shown in parenthesis.

terminal primary carbon atom are **7** (17.0 kcal mol^{-1}) and **8** (17.2 kcal mol^{-1}).

Isomer **5** is the most stable cyclic $C_2H_6S_2$ dication, lying 11.4 kcal mol^{-1} above **1a**. It presents a thiirane ring protonated at the S atom, and a SH_2^+ substituent bonded to a carbon atom. Other isomers containing a three-membered ring are **10** (20.0 kcal mol^{-1}), **12** (25.0 kcal mol^{-1}), and **14** (32.6 kcal mol^{-1}). Four-membered rings, related to the regioisomers 1,3- (**6**) and 1,2-dithiethane (**11**) protonated at both S atoms were also found, with enthalpy values of 16.7 and 23.4 kcal mol^{-1} above the **1a** structure, respectively.

Finally, only two isomers containing a disulfide bridge within a straight chain have been found. The most stable one (**9**, 19.0 kcal mol^{-1}) is related to the methyldisulfanylmethylium ion, protonated at the CH_3–S sulfur. Isomer **13**, on the other hand, is the *trans*-dimethylsulfene dication, analogous to the neutral dimethyldisulfide (DMDS) molecule. It lies 13.3 kcal mol^{-1} higher in enthalpy than its regioisomer **9**, and 30.5 kcal mol^{-1} above **1a**. Contrary to the neutral DMDS molecule, the skeleton atoms of **13** are in the same plane, in a *trans*-form configuration. Moreover, the S–S bond distance at the M06-2X/cc-pVTZ level of theory is 1.909 Å, smaller than a typical single S–S bond (2.022 Å).[57] These results suggest that the sulfur atoms of the *trans*-dimethylsulfene dication are connected by a double bond.

From these results, a qualitative analysis on the resiliency of the disulfide bridge to double ionization processes in an RSSR molecule can be made. The removal of two electrons from the S_2 moiety dramatically changes the molecular structure towards the disulfide bridge, and the RSSR dihedral angle increases from ~90° to ~180°. A similar torsional change is observed in the $CH_3SSCH_3^+$ cation, as early shown by Butler.[58] Moreover, the S–S bond length becomes shorter, and a double bond between two atoms with formal positive charges is achieved. However, while the twisted CH_3SSCH_3 and CH_3-CH_2SSH (ethyl hydrodisulfide) isomers are among the most stable neutral structures due to the presence of the strong disulfide bond, their respective doubly-charged planar structures with *trans* configuration are energetically higher than several other open chain and cyclic $C_2H_6S_2$ isomers. Therefore, a molecular reorganization of the undissociated dication is expected in order to transform the doubly-charged RSSR moiety into a more stable minimum, in which the disulfide bond is broken. Ultimately, this suggests that a substantial loss of molecular integrity should occur in the parent dication after the double ionization of DMDS, evidencing the high vulnerability of the disulfide bond with respect to oxidation. Given the importance of disulfide bonds to the three-dimensional structure of biomolecules, it seems reasonable to expect that a double ionization process could promote the breakage of the S–S bond, which will open distinct dissociation channels but also might lead to a considerable structural change in the undissociated systems. This picture is in line with previous findings by Chiang[45] and Butler,[58] which revealed that isomerization pathways preceding bond cleavage are common processes related to dissociative photoionization of DMDS in the low photon energy domain.

3.2 Ion–ion coincidences and fragmentation mechanisms

After analyzing the minimum energy structures of the $C_2H_6S_2$ dication, we focus our attention on the ion–ion coincidences and possible fragmentation mechanisms of DMDS that follow ionization from the K-shell and Auger electron release. As shown by Ankerhold *et al.*[59] for the CS_2 and OCS molecules, the ion–ion coincidence spectra contour plots do not depend on the incident energy around the sulfur K edge. We obtain similar results for the present molecule, as the *i*-variances of each *m*/*z* peak in the multivariate normal distribution analysis do not vary with the incidence energy. If the incident energy changes, differences among the PEPIPICO spectra would affect the probability of occurrence (intensity counts), but not their shape (neither the variance) within the S K-shell range. As a consequence, the same channels of ion dissociation are achieved, with variations only in their intensities.

Table 1 shows the parameters for the Coulomb explosion and the probability associated with the fragmentation of the DMDS molecule at 2465.0 eV and 2470.9 eV, following eqn (1)–(5). The mechanisms that involve the release of an H^+ ion at the beginning of the reaction were not taken into account because its low mass would not affect the overall mass balance statistically. The probability function that we pursued is related to the C and S atoms, aiming at understanding the disulfide stability. Additionally, we also performed quantum chemical calculations on selected fragmentation pathways, which were classified by their distinct overall ion coincidences. By obtaining the exoergicity of each reaction channel after calculating their ΔH^{298} values and combining these results with the statistical parameters following the work of Varas *et al.* 2015,[46] we could discriminate which are the most probable DMDS fragmentation mechanisms after the dication formation from core shell ionization. A similar approach was used by Ruhl *et al.*[60] to investigate the charge separation following double ionization of organic methyl compounds. The ΔH^{298} values are shown in Table 2. The ion–ion coincidence mass spectra of the DMDS molecule are presented in Table 1 and Fig. 3.

By inspecting Table 1, we could distinguish four probability density functions contributions that taken together account for more than 99% of the Coulomb explosion processes before the sulfur S 1s sigma resonance. These functions are related to the $[S]^+/[CH_n]^+$ ($P_{ij} = 0.704$), $[CH_n]^+/[HCS]^+$ ($P_{ij} = 0.121$), $[S]^+/[HCS]^+$ ($P_{ij} = 0.098$) and $[CH_n]^+/[SS]^+$ ($P_{ij} = 0.067$) coincidence channels. At the resonance (2470.9 eV), the probability of the doubly charged DMDS system to dissociate through the $[S]^+/[CH_n]^+$ channel increases substantially ($P_{ij} = 0.917$), while all other channels are depleted. The probability of the $[S]^+/[HCS]^+$ channel drops down to 5.1%, while $[CH_n]^+/[HCS]^+$ channel is merely 3.0%. All other channels contribute to less than 1% for the Coulomb explosion processes at the first sigma resonance. A detailed description of each one of the probability density functions is shown in the next sections.

3.2.1 The $[CH_n]^+/[S]^+$ ion coincidences. The $[CH_n]^+/[S]^+$ probability density function is dominant in both energies, accounting for around 70% ($P_{ij} = 0.704$) of the PEPIPICO spectra at 2465.0 eV and more than 90% ($P_{ij} = 0.918$) at 2470.9 eV. The fragmentation enhancement observed as one moves from a photon energy (2465.0 eV, below resonance) at which only direct photoionization processes are allowed, to a photon energy (2470.9 eV) at which a resonant process is induced, demonstrates the importance of resonant Auger processes towards the fragmentation of the molecule.[61] Furthermore, rearrangement processes observed herein are the result of extremely fast (femtosecond or attosecond regime) chemical reactions.[62] The $[CH_n]^+/[S]^+$ coincidences appear as well-defined and hydrogen-resolved islands, each one with two maximum regions, as shown in Fig. 3(a) and (d). The most intense contribution comes from the $[C]^+/[S]^+$ coincidence, followed by $[CH]^+/[S]^+$, $[CH_2]^+/[S]^+$ and $[CH_3]^+/[S]^+$. The relation of the variances for this coincidence group is 0.47 ± 0.1 (see Table 1; for details of the method, see Varas *et al.*[46]). A distinct number of mechanisms could explain the formation of such ions in coincidence. For $[C]^+/[S]^+$, the most plausible mechanism from the variance analysis is the four-body secondary decay after a deferred charge separation, as depicted in eqn (6a)–(6c).

$$C_2H_6S_2^{2+}\ (\mathbf{13}) \rightarrow CH_3CHS^{2+} + H_2S \quad (6a)$$

$$CH_3CHS^{2+} \rightarrow [S]^+ + CH_3CH^+ \quad (6b)$$

$$CH_3CH^+ \rightarrow CH_4 + [C]^+ \quad (6c)$$

Table 1 Parameters of the multivariate normal distribution function

			G_{ij}		P_{ij}	
Coincidence	μ	Σ	2465.0 eV	2470.9 eV	2465.0 eV	2470.9 eV
$[S]^+/[CH_n]^+$	$\begin{pmatrix}441\\660\end{pmatrix}$	$\begin{pmatrix}9.8 & 20.5\\20.5 & 43.9\end{pmatrix}$	62 234	12 917 950	0.704	0.918
$[CH_n]^+/[HCS]^+$	$\begin{pmatrix}456\\777\end{pmatrix}$	$\begin{pmatrix}21.5 & 20.2\\20.2 & 19.43\end{pmatrix}$	10 717	417 210	0.121	0.030
$[CH_n]^+/[SS]^+$	$\begin{pmatrix}456\\931\end{pmatrix}$	$\begin{pmatrix}32.7 & 34.8\\34.8 & 39.7\end{pmatrix}$	5968	18 558	0.067	0.001
$[CH_3]^+/[CH_nSS]^+$	$\begin{pmatrix}456\\1031\end{pmatrix}$	$\begin{pmatrix}17.8 & 17.3\\17.3 & 17.0\end{pmatrix}$	744	2568	0.008	>0.001
$[S]^+/[HCS]^+$	$\begin{pmatrix}660\\777\end{pmatrix}$	$\begin{pmatrix}18.1 & 29.8\\29.8 & 50.0\end{pmatrix}$	8703	713 342	0.098	0.051

Table 2 Heats of reactions for selected fragmentation pathways obtained at the CCSD(T)/aug-cc-pVTZ//(U)M06-2X/cc-pVTZ level

Reaction pathway	Coincidence	ΔH^{298} (kcal mol^{-1})	ΔH^{298} (eV)
$C_2H_6S_2^{2+}$ (**13**) → $C_2H_6S_2^{2+}$ (**1a**)	—	−30.5	−1.32
$C_2H_6S_2^{2+}$ (**13**) → S^+ (^{4}S) + C^+ (^{2}P) + CH_4 + H_2S	$[S]^+/[C]^+$	183.1	7.94
$C_2H_6S_2^{2+}$ (**13**) → S^+ (^{4}S) + C^+ (^{2}P) + CH_3SH + H_2	$[S]^+/[C]^+$	200.7	8.70
$C_2H_6S_2^{2+}$ (**13**) → S^+ (^{4}S) + CH^+ + CH_4 + SH	$[S]^+/[CH]^+$	179.2	7.77
$C_2H_6S_2^{2+}$ (**13**) → S^+ (^{4}S)$^+$ CH^+ + CH_3S + H_2	$[S]^+/[CH]^+$	192.3	8.34
$C_2H_6S_2^{2+}$ (**13**) → S^+ (^{4}S) + CH^+ + CH_3 + H_2S	$[S]^+/[CH]^+$	193.2	8.38
$C_2H_6S_2^{2+}$ (**13**) → S^+ (^{4}S) + CH^+ + CH_3SH + H (^{2}S)	$[S]^+/[CH]^+$	210.5	9.13
$C_2H_6S_2^{2+}$ (**13**) → S^+ (^{4}S) + CH_2^+ + CH_3SH	$[S]^+/[CH_2]^+$	105.4	4.57
$C_2H_6S_2^{2+}$ (**13**) → S^+ (^{4}S) + CH_2^+ + H_2CS + H_2	$[S]^+/[CH_2]^+$	139.9	6.07
$C_2H_6S_2^{2+}$ (**13**) → S^+ (^{4}S) + CH_2^+ + CH_4 + S (^{3}P)	$[S]^+/[CH_2]^+$	156.1	6.77
$C_2H_6S_2^{2+}$ (**13**) → S^+ (^{4}S) + CH_2^+ + CH_3 + SH	$[S]^+/[CH_2]^+$	177.5	7.70
$C_2H_6S_2^{2+}$ (**13**) → S^+ (^{4}S) + CH_2^+ + CH_2 + H_2S	$[S]^+/[CH_2]^+$	197.1	8.55
$C_2H_6S_2^{2+}$ (**13**) → S^+ (^{4}S) + CH_3^+ + CH_3S	$[S]^+/[CH_3]^+$	69.0	2.99
$C_2H_6S_2^{2+}$ (**13**) → S^+ (^{4}S) + CH_3^+ + H_2CS + H (^{2}S)	$[S]^+/[CH_3]^+$	121.6	5.27
$C_2H_6S_2^{2+}$ (**13**) → S^+ (^{4}S) + CH_3^+ + CH_3 + S	$[S]^+/[CH_3]^+$	138.2	5.99
$C_2H_6S_2^{2+}$ (**13**) → S^+ (^{4}S) + CH_3^+ + CH_2 + SH	$[S]^+/[CH_3]^+$	165.1	7.16
$C_2H_6S_2^{2+}$ (**13**) → S^+ (^{4}S) + CH_3^+ + CH + H_2S	$[S]^+/[CH_3]^+$	175.1	7.59
$C_2H_6S_2^{2+}$ (**13**) → S^+ (^{4}S) + HCS^+ + H (^{2}S) + CH_4	$[S]^+/[HCS]^+$	58.9	2.55
$C_2H_6S_2^{2+}$ (**13**) → S^+ (^{4}S) + HCS^+ + H_2 + CH_3	$[S]^+/[HCS]^+$	59.2	2.57
$C_2H_6S_2^{2+}$ (**13**) → CH_2^+ + HCS^+ + SH + H_2	$[CH_2]^+/[HCS]^+$	90.2	3.91
$C_2H_6S_2^{2+}$ (**13**) → CH_2^+ + HCS^+ + H_2S + H (^{2}S)	$[CH_2]^+/[HCS]^+$	103.8	4.50
$C_2H_6S_2^{2+}$ (**13**) → CH_3^+ + HCS^+ + H_2S	$[CH_3]^+/[HCS]^+$	−17.5	−0.76
$C_2H_6S_2^{2+}$ (**13**) → CH_3^+ + HCS^+ + H_2 + S (^{3}P)	$[CH_3]^+/[HCS]^+$	50.8	2.20
$C_2H_6S_2^{2+}$ (**13**) → CH_3^+ + HCS^+ + H (^{2}S) + SH	$[CH_3]^+/[HCS]^+$	71.9	3.12
$C_2H_6S_2^{2+}$ (**13**) → CH_3^+ + S_2^+ + CH_3	$[CH_3]^+/[S_2]^+$	26.1	1.13
$C_2H_6S_2^{2+}$ (**13**) → CH_3^+ + S_2^+ + CH + H_2	$[CH_3]^+/[S_2]^+$	131.4	5.70
$C_2H_6S_2^{2+}$ (**13**) → CH_3^+ + S_2^+ + CH_2 + H	$[CH_3]^+/[S_2]^+$	135.1	5.86
$C_2H_6S_2^{2+}$ (**13**) → CH_3^+ + $CH_3S_2^+$	$[CH_3]^+/[CH_3S_2]^+$	−37.9	−1.64
$C_2H_6S_2^{2+}$ (**13**) → $2SCH_3^+$	$[SCH_3]^+/[SCH_3]^+$	0.8	0.03
$C_2H_6S_2^{2+}$ (**13**) → S^+ (^{4}S) + S^+ (^{4}S) + C_2H_6	$[S]^+/[S]^+$	58.4	2.53

In the first step, there is a release of neutral H_2S, and the remaining doubly-charged $[CH_3CHS]^{2+}$ species is then dissociated into $[S]^+$ and $[CH_3CH]^+$. The latter ion finally decomposes into CH_4 and $[C]^+$. This mechanism is also supported by our thermochemistry calculations, which revealed that the formation of neutral CH_4 and H_2S as a consequence of dissociation from $DMDS^{2+}$ is the least endoergic pathway (7.94 eV) associated to the $[C]^+/[S]^+$ coincidence. Similar mechanisms could be proposed for the other CH_n^+ ions, as shown in eqn (7)–(9):

$$C_2H_6S_2^{2+}\ (\mathbf{13}) \rightarrow CH_3CHS^{2+} + H_2S \quad (7a)$$

$$CH_3CHS^{2+} \rightarrow [S]^+ + CH_3CH^+ \quad (7b)$$

$$CH_3CH^+ \rightarrow CH_3 + [CH]^+ \quad (7c)$$

$$C_2H_6S_2^{2+}\ (\mathbf{13}) \rightarrow CH_3CH_2S^{2+} + SH \quad (8a)$$

$$CH_3CH_2S^{2+} \rightarrow [S]^+ + CH_3CH_2^+ \quad (8b)$$

$$CH_3CH_2^+ \rightarrow CH_3 + [CH_2]^+ \quad (8c)$$

$$C_2H_6S_2^{2+}\ (\mathbf{13}) \rightarrow CH_3CH_2SH^{2+} + S \quad (9a)$$

$$CH_3CH_2SH^{2+} \rightarrow [S]^+ + CH_3CH_3^+ \quad (9b)$$

$$CH_3CH_3^+ \rightarrow CH_3 + [CH_3]^+ \quad (9c)$$

To the best of our knowledge, H_2S or SH dissociation from a doubly-charged DMDS molecule has not been studied computationally up to date. Different fragmentation routes for neutral SH loss from the monocationic DMDS species, however, have been described by Borkar and coworkers.[43] From their results, the least endergonic pathway involves initial methyl migration to form an $SS(CH_3)_2^+$ intermediate, followed by C–H activation of one of the hydrogen atoms of the methyl group by the terminal S atom. The S–S bond of the $HSS(CH_2)(CH_3)^+$ intermediate is then cleaved, leading to neutral SH and $CH_2SCH_3^+$. As none of these intermediates were found for the dication, our results suggest that this particular route is not allowed for the doubly-charged DMDS molecule. On the other hand, both the global minimum **1a** and most of the low-lying isomers possess terminal H_2S groups, indicating that these are all suitable structures for further fragmentation through H_2S loss.

The mechanisms depicted in eqn (6) and (7) are also in agreement with the previous work by Butler,[58] which observed that the release of neutral S species competes with the direct H_3CS–SCH_3 bond cleavage. The enthalpies of these fragmentation pathways are 7.77 eV, 6.77 eV and 5.99 eV, respectively. For the $[CH]^+/[S]^+$ coincidence the depicted pathway is also the least

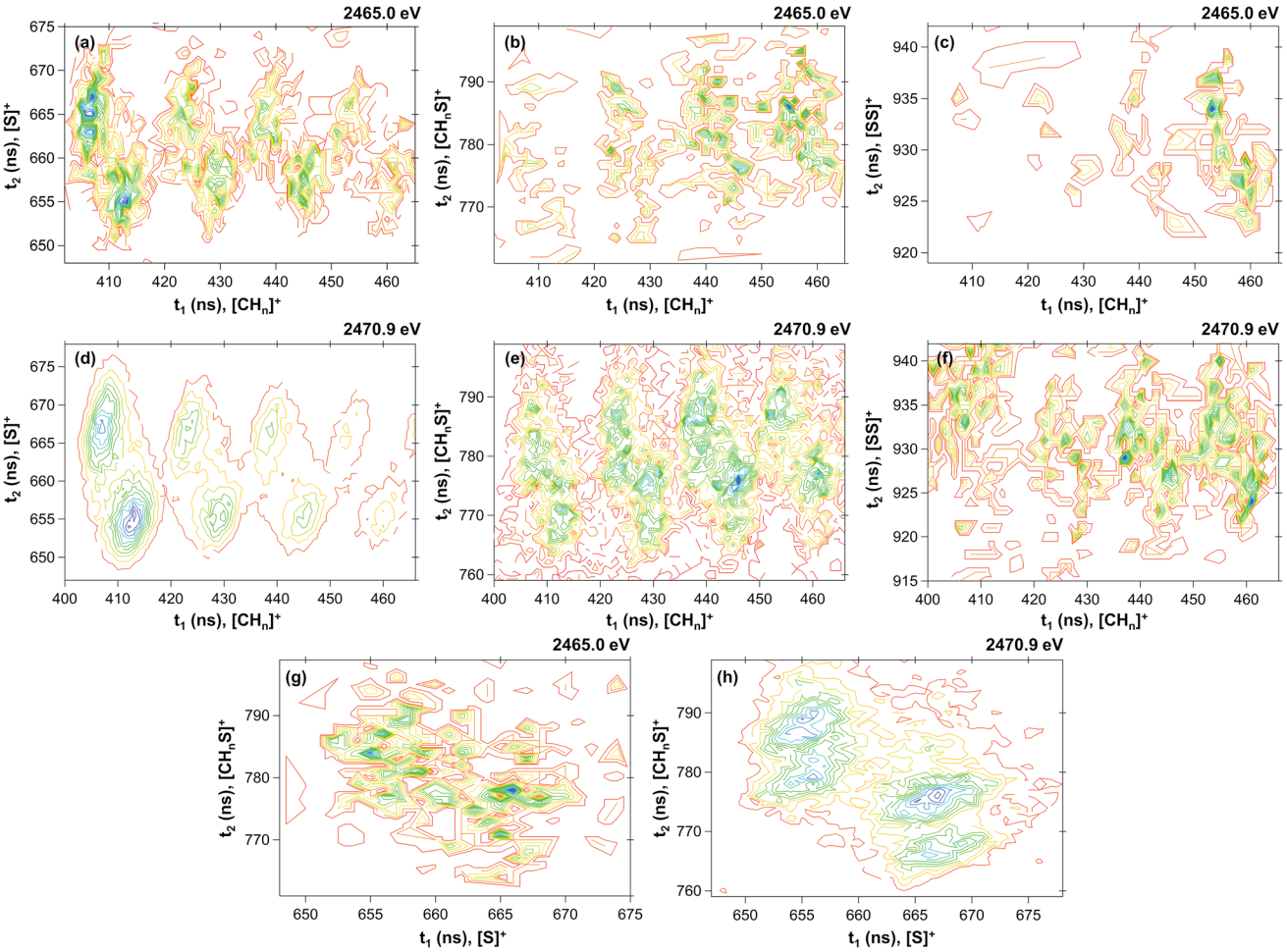

Fig. 3 Contour plot of coincidence islands at 2465.0 eV ((a) $[CH_n]^+/[S]^+$; (b) $[CH_n]^+/[CH_nS]^+$; (c) $[CH_n]^+/[SS]^+$; (g) $[S]^+/[CH_nS]^+$) and at 2470.9 eV ((d) $[CH_n]^+/[S]^+$; (e) $[CH_n]^+/[CH_nS]^+$; (f) $[CH_n]^+/[SS]^+$; (h) $[S]^+/[CH_nS]^+$).

endoergic one, as revealed by the thermochemistry calculations. However, this is not the case for the $[CH_n]^+/[S]^+$ coincidences related to the $[CH_2]^+$ and $[CH_3]^+$ ions, where the most stable pathways are three-body dissociations that involve the formation of only one neutral species. The relation of the variances suggests that three-body secondary decay processes could also occur for the $[CH_n]^+/[S]^+$, leading to the following set of equations:

$$C_2H_6S_2^{2+}\ (\mathbf{13}) \rightarrow [CH_3]^+ + CH_3SS^+ \quad (10a)$$

$$CH_3SS^+ \rightarrow [S]^+ + CH_3S \quad (10b)$$

$$C_2H_6S_2^{2+}\ (\mathbf{13}) \rightarrow [CH_2]^+ + CH_3SSH^+ \quad (11a)$$

$$CH_3SSH^+ \rightarrow [S]^+ + CH_3SH \quad (11b)$$

The homolytic charge dissociation of the doubly-charged DMDS molecule leading to $[CH_3]^+$ and $[CH_3SS]^+$ is the most stable fragmentation pathway as revealed by our calculations, being exoergic by -37.9 kcal mol^{-1} (-1.64 eV). This comes from the fact that the C–S bond is weaker than the S–S bond in DMDS,[63] and also could explain the high yields of the $[CH_3SS]^+$ ion in mass spectra of valence ionization processes.[64] Taken together, our results suggest that the main fragmentation mechanism leading to $[C]^+$ and $[CH]^+$ are processes related to four-body secondary decay after a deferred charge separation, while $[CH_2]^+$ and $[CH_3]^+$ are formed mainly through a three-body secondary decay.

3.2.2 The $[CH_n]^+/[HCS]^+$ ion coincidence. The $[CH_n]^+/[HCS]^+$ probability density function accounts for around 12% of the PEPIPICO spectra at 2465.0 eV and merely 3% at 2470.9 eV. As in the previous case, these coincidences are observed as well-defined and hydrogen-resolved islands, each one also presenting two maximum regions, as shown in Fig. 3(b) and (e). The most intense contribution comes from the $[CH_2]^+/[S]^+$ and $[CH_3]^+/[S]^+$ coincidences, and the relation of the variances for the group is 0.94 ± 0.1 (see Table 1). This value, in combination to the thermochemistry calculations, suggests the mechanisms depicted in eqn (12) and (13), which are also related to a four-body secondary decay after a deferred charge separation:

$$C_2H_6S_2^{2+}\ (\mathbf{13}) \rightarrow CH_3SCH_2^{2+} + SH \quad (12a)$$

$$CH_3SCH_2^{2+} \rightarrow CH_3S^+ + [CH_2]^+ \quad (12b)$$

$$CH_3S^+ \rightarrow [HCS]^+ + H_2 \quad (12c)$$

$$C_2H_6S_2^{2+}\ (\mathbf{13}) \rightarrow CH_3SCH_3^{2+} + S \quad (13a)$$

$$CH_3SCH_3^{2+} \rightarrow CH_3S^+ + [CH_3]^+ \quad (13b)$$

$$CH_3S^+ \rightarrow [HCS]^+ + H_2 \quad (13c)$$

The enthalpy value for the first mechanism is 3.91 eV, while for the latter is 2.20 eV. A three-body dissociation into $[CH_3]^+$, $[HCS]^+$ and H_2S is exoergic by −17.5 kcal mol^{-1} (−0.76 eV), suggesting that it could also be a relevant dissociation pathway.

3.2.3 The $[S]^+/[HCS]^+$ ion coincidence. The $[S]^+/[HCS]^+$ probability density function is the third most important contribution for the PEPIPICO spectra at 2465.0 eV, accounting for around 10% of the overall coincidences. At the first sigma resonance, its contribution lowers to 5%, being then the second most relevant coincidence at 2470.9 eV. The coincidence islands at both energies are shown in Fig. 3(g) and (h). The relation of the variances is 0.60 ± 0.1, which leads to the following mechanism:

$$C_2H_6S_2^{2+}\ (\mathbf{13}) \rightarrow CH_3SSCH_2^{2+} + H \quad (14a)$$

$$CH_3SSCH_2^{2+} \rightarrow [HCS]^+ + CH_3SH^+ \quad (14b)$$

$$CH_3SH^+ \rightarrow [S]^+ + CH_4 \quad (14c)$$

Or, analogously:

$$C_2H_6S_2^{2+}\ (\mathbf{13}) \rightarrow CH_3SSCH^{2+} + H_2 \quad (15a)$$

$$CH_3SSCH^{2+} \rightarrow [HCS]^+ + CH_3S^+ \quad (15b)$$

$$CH_3S^+ \rightarrow [S]^+ + CH_3 \quad (15c)$$

The enthalpy values for the dissociation pathways are 58.9 kcal mol^{-1} (2.55 eV) and 59.2 kcal mol^{-1} (2.57 eV), respectively. Therefore, the calculations suggest that both mechanisms seem plausible for accounting to the $[S]^+/[HCS]^+$ coincidence.

3.2.4 The $[CH_n]^+/[SS]^+$ ion coincidence. The $[CH_n]^+/[SS]^+$ probability density function has the smallest contribution among the ones described herein. It accounts for less than 1% in both energies. At 2465.0 eV (Fig. 3(c)), only contributions coming from the $[CH_3]^+/[SS]^+$ are observed, while less pronounced coincidence islands from $[CH_2]^+/[SS]^+$, $[CH]^+/[SS]^+$ and $[C]^+/[SS]^+$ are also obtained at 2470.9 eV (Fig. 3(f)). The following mechanism is proposed for the $[CH_3]^+/[SS]^+$ coincidence:

$$C_2H_6S_2^{2+}\ (\mathbf{13}) \rightarrow CH_3SS^{2+} + CH_3 \quad (16a)$$

$$CH_3SS^{2+} \rightarrow [CH_3]^+ + [SS]^+ \quad (16b)$$

With the electron gun at 800 eV,[46] the most probable dissociation channel involves the formation of the CH_3SS^+ ion, which contains a disulfide bond. The main differences between the low-energy fragmentation studies and those presented herein are related to the nature of the inelastic collisions (electrons losing energy and producing valence ionization instead of inner-shell processes) as well as the energy absorbed by the molecule after the ionization. As a consequence, it is expected that these processes will give rise to distinct molecular fragmentation channels, and also to distinct fragment branching ratios. For valence ionization, the most probable double coincidence channels for DMDS are related to the $[CH_3SS]^+/[CH_3]^+$ and $[CH_3]^+/[SS]^+$, whereas for inner-shell ionization the yields of fragments containing the S_2 moiety are negligible.

Chemical bonding is usually thought as being solely related to valence electrons, with core electrons playing only a minor role. Conversely, a vast body of literature has demonstrated that the excitation and ionization of core electrons may lead to an extensive breakage of chemical bonds, and consequently to molecular dissociation.[65–67] However, the effectiveness of bond breaking after inner-shell excitation depends not only on the impact energies and the nature of the atom that is being ionized, but also on the chemical bond itself. By comparing the yields of the fragmentation products of DMDS after ionization using photon energies around the sulfur K-shell resonance obtained herein, it is possible to see that the S–S bond is significantly more affected than the C–S bond, as S_2-bearing fragments are negligible. This trend is the opposite than what is expected from the corresponding bond strengths, as the S–S bond in DMDS is stronger than C–S.[63] Additionally, our calculations reveal that the global minimum and the low-lying isomers of the doubly-charged parent ion with $C_2H_6S_2$ stoichiometry do not present disulfide bonding, indicating that their stabilizing effect is severely weakened after double ionization. Taken together, these results evidence that the S–S bond is not stable enough to compensate for a double ionization event, and that any parent DMDS dication that may avoid fragmentation should undergo a severe isomerization process and loss of structural integrity during the time-of-flight.

4 Conclusions

In summary, we studied the resilience of the disulfide bond in the dimethyl disulfide (DMDS) molecule subjected to doubly ionization process combining coincidence spectroscopy and quantum chemical calculations. Initially, we mapped the minimum energy structures of the $C_2H_6S_2^{2+}$ dication, and showed that, in contrast to their analogous neutral systems, disulfide bonds are only present in high-lying isomers. The global minimum (**1**) at the CCSD(T)/aug-cc-pVTZ//M06-2X/cc-pVTZ level of theory is the protonated dimercaptoethanylium system, which contains terminal H_2S^+ and HS^+ groups. In opposition to neutral DMDS, the doubly-charged $CH_3SSCH_3^{2+}$ system (**13**) presents a planar backbone and a short S–S bond of merely 1.909 Å, and the resulting structure is 30.5 kcal mol^{-1} less stable than **1**. By using a multivariate normal distribution protocol, we were able to discriminate the most plausible fragmentation mechanisms that contribute to the two-dimensional photoelectron–photoion–photoion coincidence (PEPIPICO) spectra of DMDS following photon impact with energies around the S 1s resonance. Furthermore, we showed that the branching

ratios of DMDS fragmentation with high energy photons are dependent on whether the hole is created in resonance or not. Our results revealed that the disulfide bond is severely damaged as a consequence of sulfur core–shell ionization processes, and this is related to the low thermodynamic stability of such a bonding in multiply-charged systems. Further double fragmentation experiments are being conducted for the dimethyl sulfide (DMS) and methyl propyl disulfide (MPDS) molecules.

Conflicts of interest

There are no conflicts to declare.

Acknowledgements

The authors acknowledge CNPq, CAPES, Universidad de Costa Rica and FAPERJ for financial support. We are grateful to the Brazilian Synchrotron Light Facility (LNLS) for financial and technical assistance. We are particularly indebted to Tamires M. Gallo, Flavio Vicentin and Paulo T. Fonseca for their help during the course of the experiments. F. F. acknowledges CAPES and the Alexander von Humboldt Foundation for a Capes-Humboldt fellowship for postdoctoral researchers.

References

1 J. Holdship, I. Jimenez-Serra, S. Viti, C. Codella, M. Benedettini, F. Fontani, M. Tafalla, R. Bachiller, C. Ceccarelli and L. Podio, *Astrophys. J.*, 2019, **878**, 64.
2 R. Le Gal, K. I. Öberg, R. A. Loomis, J. Pegues and J. B. Bergner, *Astrophys. J.*, 2019, **876**, 72.
3 J. R. Goicoechea, J. Pety, M. Gerin, D. Teyssier, E. Roueff, P. Hily-Blant and S. Baek, *Astron. Astrophys.*, 2006, **456**, 565–580.
4 P. P. B. Beaklini, E. Mendoza, C. M. Canelo, I. Aleman, M. Merello, S. Kong, F. Navarete, E. Janot-Pacheco, Z. Abraham, J. R. D. Lépine, A. A. de Almeida and A. C. S. Friaça, *Mon. Not. R. Astron. Soc.*, 2020, **491**, 427–439.
5 S. Maity and R. I. Kaiser, *Astrophys. J.*, 2013, **773**, 184.
6 A. Ruf, A. Bouquet, P. Boduch, P. Schmitt-Kopplin, V. Vinogradoff, F. Duvernay, R. G. Urso, R. Brunetto, L. Le Sergeant d'Hendecourt, O. Mousis and G. Danger, *Astrophys. J.*, 2019, **885**, L40.
7 X. Zhang, M. C. Liang, F. P. Mills, D. A. Belyaev and Y. L. Yung, *Icarus*, 2012, **217**, 714–739.
8 V. A. Krasnopolsky, *Icarus*, 2016, **274**, 33–36.
9 P. Schmitt-Kopplin, Z. Gabelica, R. D. Gougeon, A. Fekete, B. Kanawati, M. Harir, I. Gebefuegi, G. Eckel and N. Hertkorn, *Proc. Natl. Acad. Sci. U. S. A.*, 2010, **107**, 2763–2768.
10 E. T. Parker, H. J. Cleaves, M. P. Callahan, J. P. Dworkin, D. P. Glavin, A. Lazcano and J. L. Bada, *Origins Life Evol. Biospheres*, 2011, **41**, 569–574.
11 E. T. Parker, H. J. Cleaves, J. P. Dworkin, D. P. Glavin, M. Callahan, A. Aubrey, A. Lazcano and J. L. Bada, *Proc. Natl. Acad. Sci. U. S. A.*, 2011, **108**, 5526–5531.
12 G. Wächtershäuser, *Prog. Biophys. Mol. Biol.*, 1992, **58**, 85–201.
13 G. Wachtershauser, *Science*, 2000, **289**, 1307–1308.
14 J. Thiel, J. M. Byrne, A. Kappler, B. Schink and M. Pester, *Proc. Natl. Acad. Sci. U. S. A.*, 2019, **116**, 6897–6902.
15 B. Meyer, *Chem. Rev.*, 1976, **76**, 367–388.
16 R. Steudel and B. Eckert, *Elem. Sulfur Sulfur-Rich Compd. I. Top. Curr. Chem.*, Springer, Berlin, Heidelberg, 230th edn, 2003, pp. 1–79.
17 D. Hohl, R. O. Jones, R. Car and M. Parrinello, *J. Chem. Phys.*, 1988, **89**, 6823–6835.
18 K. Raghavachari, C. M. Rohlfing and J. S. Binkley, *J. Chem. Phys.*, 1990, **93**, 5862–5874.
19 R. O. Jones and P. Ballone, *J. Chem. Phys.*, 2003, **118**, 9257–9265.
20 R. Gleiter, G. Haberhauer and F. Rominger, *Eur. J. Inorg. Chem.*, 2019, **2019**, 3846–3853.
21 G. D. Brabson, Z. Mielke and L. Andrews, *J. Phys. Chem.*, 1991, **95**, 79–86.
22 R. Steudel, O. Schumann, J. Buschmann and P. Luger, *Angew. Chem., Int. Ed.*, 1998, **37**, 2377–2378.
23 R. Steudel, J. Steidel, J. Pickardt, F. Schuster and R. Reinhardt, *Z. Naturforsch., B: Anorg. Chem., Org. Chem.*, 1980, **35**, 1378–1383.
24 S. Matsuno, M. Yamashina, Y. Sei, M. Akita, A. Kuzume, K. Yamamoto and M. Yoshizawa, *Nat. Commun.*, 2017, **8**, 749.
25 R. Steudel, R. Strauss and L. Koch, *Angew. Chem., Int. Ed. Engl.*, 1985, **24**, 59–60.
26 R. Ludwig, J. Behler, B. Klink and F. Weinhold, *Angew. Chem., Int. Ed.*, 2002, **41**, 3199–3202.
27 H. Beinert, *Science*, 1997, **277**, 653–659.
28 J. Liu, S. Chakraborty, P. Hosseinzadeh, Y. Yu, S. Tian, I. Petrik, A. Bhagi and Y. Lu, *Chem. Rev.*, 2014, **114**, 4366–4469.
29 A. Fuente, J. R. Goicoechea, J. Pety, R. Le Gal, R. Martín-Doménech, P. Gratier, V. Guzmán, E. Roueff, J. C. Loison, G. M. Muñoz Caro, V. Wakelam, M. Gerin, P. Riviere-Marichalar and T. Vidal, *Astrophys. J.*, 2017, **851**, L49.
30 R. C. Fortenberry and J. S. Francisco, *Astrophys. J.*, 2018, **856**, 30.
31 S. F. Betz, *Protein Sci.*, 1993, **2**, 1551–1558.
32 W. J. Wedemeyer, E. Welker, M. Narayan and H. A. Scheraga, *Biochemistry*, 2000, **39**, 4207–4216.
33 B. Schmidt, L. Ho and P. J. Hogg, *Biochemistry*, 2006, **45**, 7429–7433.
34 M. Trivedi, J. Laurence and T. Siahaan, *Curr. Protein Pept. Sci.*, 2009, **10**, 614–625.
35 N. Samainukul, A. K. Linn, M. B. Javadi, S. Sakdee, C. Angsuthanasombat and G. Katzenmeier, *Biochem. Biophys. Res. Commun.*, 2019, **514**, 365–371.
36 H. Kadokura, F. Katzen and J. Beckwith, *Annu. Rev. Biochem.*, 2003, **72**, 111–135.
37 I. Dragičević, D. Barić, B. Kovačević, B. T. Golding and D. M. Smith, *Chem.–Eur. J.*, 2015, **21**, 6132–6143.
38 G. G. B. de Souza and J. C. Gonzalez, *Radiat. Bioanal.*, Springer, Cham, 8th edn, 2019, pp. 287–312.

39 R. B. Bernini, L. B. G. da Silva, F. N. Rodrigues, L. H. Coutinho, A. B. Rocha and G. G. B. de Souza, *J. Chem. Phys.*, 2012, **136**, 144307.
40 J. Gonzalez, G. Simões, R. Bernini, L. Coutinho, F. Stedile, C. Nunez, F. Vicentin and G. de Souza, *J. Braz. Chem. Soc.*, 2019, **30**, 1887–1896.
41 G. Simões, F. Rodrigues, R. Bernini, C. Castro and G. de Souza, *J. Electron Spectrosc. Relat. Phenom.*, 2014, **193**, 21–26.
42 R. C. M. Salles, L. H. Coutinho, A. G. da Veiga, M. M. Sant'Anna and G. G. B. de Souza, *J. Chem. Phys.*, 2018, **148**, 045107.
43 S. Borkar, B. Sztáray and A. Bodi, *J. Electron Spectrosc. Relat. Phenom.*, 2014, **196**, 165–172.
44 J. J. Butler, T. Baer and S. A. Evans, *J. Am. Chem. Soc.*, 1983, **105**, 3451–3455.
45 S.-Y. Chiang, C.-I. Ma and D.-J. Shr, *J. Chem. Phys.*, 1999, **110**, 9056–9063.
46 L. R. Varas, F. C. Pontes, A. C. F. Santos, L. H. Coutinho and G. G. B. de Souza, *Rapid Commun. Mass Spectrom.*, 2015, **29**, 1571–1576.
47 L. Fransinski, K. Codling and P. Hatherly, *Phys. Lett. A*, 1989, **142**, 499–503.
48 J. Eland, *Mol. Phys.*, 1987, **61**, 725–745.
49 L. R. Varas, L. H. Coutinho, R. B. Bernini, A. M. Betancourt, C. E. V. de Moura, A. B. Rocha and G. G. B. de Souza, *RSC Adv.*, 2017, **7**, 36525–36532.
50 L. J. Frasinski, M. Stankiewicz, K. J. Randall, P. A. Hatherly and K. Codling, *J. Phys. B: At. Mol. Phys.*, 1986, **19**, L819–L824.
51 M. Lavollée and V. Brems, *J. Chem. Phys.*, 1999, **110**, 918–926.
52 M. Simon, T. Lebrun, R. Martins, G. G. B. de Souza, I. Nenner, M. Lavollee and P. Morin, *J. Phys. Chem.*, 1993, **97**, 5228–5237.
53 E. W. Weisstein, *Gaussian function*, 2002.
54 F. Burmeister, L. Coutinho, R. Marinho, M. Homem, M. De Morais, A. Mocellin, O. Björneholm, S. Sorensen, P. d. T. Fonseca, A. Lindgren, *et al.*, *J. Electron Spectrosc. Relat. Phenom.*, 2010, **180**, 6–13.
55 M. J. Frisch, G. W. Trucks, H. B. Schlegel, G. E. Scuseria, M. A. Robb, J. R. Cheeseman, G. Scalmani, V. Barone, G. A. Petersson, H. Nakatsuji, X. Li, M. Caricato, A. V. Marenich, J. Bloino, B. G. Janesko, R. Gomperts, B. Mennucci, H. P. Hratchian, J. V. Ortiz, A. F. Izmaylov, J. L. Sonnenberg, D. Williams-Young, F. Ding, F. Lipparini, F. Egidi, J. Goings, B. Peng, A. Petrone, T. Henderson, D. Ranasinghe, V. G. Zakrzewski, J. Gao, N. Rega, G. Zheng, W. Liang, M. Hada, M. Ehara, K. Toyota, R. Fukuda, J. Hasegawa, M. Ishida, T. Nakajima, Y. Honda, O. Kitao, H. Nakai, T. Vreven, K. Throssell, J. A. Montgomery Jr, J. E. Peralta, F. Ogliaro, M. J. Bearpark, J. J. Heyd, E. N. Brothers, K. N. Kudin, V. N. Staroverov, T. A. Keith, R. Kobayashi, J. Normand, K. Raghavachari, A. P. Rendell, J. C. Burant, S. S. Iyengar, J. Tomasi, M. Cossi, J. M. Millam, M. Klene, C. Adamo, R. Cammi, J. W. Ochterski, R. L. Martin, K. Morokuma, O. Farkas, J. B. Foresman and D. J. Fox, *Gaussian 16 Revision C.01*, Gaussian Inc., Wallingford CT, 2016.
56 S. Grimme, M. Steinmetz and M. Korth, *J. Org. Chem.*, 2007, **72**, 2118–2126.
57 B. Beagley and K. T. McAloon, *Trans. Faraday Soc.*, 1971, **67**, 3216.
58 J. J. Butler, T. Baer and S. A. Evans Jr, *J. Am. Chem. Soc.*, 1983, **105**, 3451–3455.
59 U. Ankerhold, B. Esser and F. von Busch, *J. Phys. B: At., Mol. Opt. Phys.*, 1997, **30**, 1207–1222.
60 E. Ruhl, S. Price, S. Leach and J. Eland, *J. Phys. B: At., Mol. Opt. Phys.*, 1990, **97**, 175–201.
61 M. Piancastelli, *J. Electron Spectrosc. Relat. Phenom.*, 2000, **107**, 1–26.
62 T. Marchenko, S. Carniato, L. Journel, R. Guillemin, E. Kawerk, M. Žitnik, M. Kavčič, K. Bučar, R. Bohinc, M. Petric, *et al.*, *Phys. Rev. X*, 2015, **5**, 031021.
63 S. W. Benson, *Chem. Rev.*, 1978, **78**, 23–35.
64 S. Stein, *NIST/EPA/NIH Mass Spectral Library with Search Program, NIST Standard Reference Database 1A*, 2005.
65 I. Nenner and P. Morin, *VUV and Soft X-ray Photoionization* ed U. Becker and D. A. Shirley, 1996.
66 R. Feifel and M. N. Piancastelli, *J. Electron Spectrosc. Relat. Phenom.*, 2011, **183**, 10–28.
67 M. Quack and F. Merkt, *Handbook of high-resolution spectroscopy*, Wiley-Blackwell, 2011.

